

Structural and Thermal Behavior of Fe-Cr-Mo-P-B-C-Si Amorphous and Nanocrystalline HVOF Coatings

B. Movahedi, M.H. Enayati, and C.C. Wong

(Submitted January 4, 2010; in revised form March 31, 2010)

The microstructure, thermal behavior, and mechanical properties of amorphous/nanocrystalline 70Fe-15Cr-4Mo-5P-4B-1C-1Si (wt.%) coatings produced by high velocity oxy fuel (HVOF) spraying of mechanically alloyed powders were investigated by x-ray diffractometry (XRD), scanning electron microscopy (SEM), and transmission electron microscopy (TEM). Thermal stability of samples was investigated using differential scanning calorimetry (DSC). The results show that by adjusting the HVOF parameters especially fuel/oxygen ratio and proper selection of powder composition, the desired microstructure with different amount of amorphous and nanocrystalline phases and therefore with different mechanical properties could be obtained.

Keywords amorphous, Fe-base, HVOF, mechanical alloying, nanocrystalline

1. Introduction

Synthesizing amorphous and/or nanocrystalline layers on metal substrates can be utilized to improve surface performance such as wear and corrosion resistance (Ref 1). Greer et al. reported that amorphous alloys can have very good resistance to sliding and abrasive wear and the coatings can have low friction coefficient (Ref 2). Thermal spraying process is one of the techniques to deposit amorphous coatings on surfaces, where the amorphous structure is retained due to the sufficiently rapid cooling that inhibits long-range diffusion and crystallization. On impact with the substrate, droplet spreading occurs to give lamellar morphologies with cooling rates of 10^7 - 10^8 K/s (Ref 3). A number of researchers have investigated the use of air plasma spraying (APS), low pressure plasma spraying (LPPS) and vacuum plasma spraying (VPS) to deposit alloys, which are capable of solidifying as metallic glasses (Ref 4, 5). Kishitake et al. reported that mixed amorphous and crystalline structures

are obtained in APS and LPPS coatings (Ref 5, 6). In recent years, there has been an increasing interest in the use of high velocity oxy-fuel (HVOF) thermal spraying for depositing protective coatings. In the HVOF process, the flame temperature is moderate (\approx 3000 °C) while the velocity of the powder particles is very high (850 m/s). The favorable properties given by HVOF process include low porosity (less 1%), high hardness (40-70 HRC), low oxide contents, high adhesion (>70 MPa), and compressive stress in coating (Ref 3, 7).

During the HVOF process, melting of the alloy powders occurs in the flame. The droplets rapidly solidify with a high cooling rate upon their impact onto the substrate. However, there is a certain composition range where the amorphous phase can be stabilized against the precipitation of the crystalline phase. The general methodology involves designing alloys that have low critical cooling rates for glass formation. Alloys with high glass forming ability (GFA) would be favorable for forming fully amorphous phase coating by HVOF process. Recently, a number of Fe-based bulk metallic glasses with good GFA were found in the Fe-(Cr, Mo)-(C, B) system. The critical cooling rate for glass formation of $Fe_{43}Cr_{16}Mo_{16}(C, B, P)_{25}$ system synthesized by copper mold casting is evaluated to be of the order of 10^2 K/s (Ref 8-10). The phase composition (i.e., the concentration of interstitial solute atoms such as B, C, P, and Si) could play an important role in amorphization (Ref 11-13).

The amorphous coatings, while exhibiting interesting properties, can be heated up above their crystallization temperature to initiate devitrification and yield amorphous-crystalline mixture. Since the driving force for the crystallization is extremely high and the diffusion rate in the solid state, at the crystallization temperature, is very low, an extremely high nucleation frequency results. There is limited time for growth before impingement between neighboring crystallites occurs, resulting in the formation of nanoscale microstructures (Ref 14-18).

B. Movahedi, Department of Materials Engineering, Isfahan University of Technology, Isfahan 84156 83111, Iran and School of Materials Science and Engineering, Nanyang Technological University, Nanyang Avenue, Singapore 639798, Singapore; **M.H. Enayati**, Department of Materials Engineering, Isfahan University of Technology, Isfahan 84156 83111, Iran and Poudrafshan Company (PACO), Isfahan Science and Technology Town (ISTT), Isfahan, Iran; and **C.C. Wong**, School of Materials Science and Engineering, Nanyang Technological University, Nanyang Avenue, Singapore 639798, Singapore. Contact e-mails: b_movahedy@yahoo.com and movahedi@ma.iut.ac.ir.

In previous works (Ref 4-6, 14, 19), the formation of Fe-base amorphous coatings by LPPS, high-energy plasma spraying (HPS), and HVOF processes were studied with using atomized feedstock powder. The goal of the present work is to produce at first amorphous mechanical alloying feedstock powder and then amorphous-nanocrystalline coatings in a new composition 70Fe-15Cr-4Mo-5P-4B-1C-1Si (wt.%) by HVOF process and to study the properties of resulting structure. This alloy includes four types of elements: late transition metal (Fe), early transition metals (Cr, Mo), metalloids (B, P, Si), and graphite. The atomic radius of the constituent elements decreases as Mo (0.139 nm) > Si (0.132 nm) > P (0.128 nm) > Cr (0.127 nm) > Fe (0.126 nm) > B (0.098 nm) > C (0.091 nm). The heats of mixing are negative for the atomic pairs of Fe-(Cr, Mo), (Cr, Mo)-(B, P, Si), and Fe-(B, P, Si) (Ref 8). These properties suggest that 70Fe-15Cr-4Mo-5P-4B-1C-1Si (wt.%) composition has a high GFA and thermal stability (Ref 20).

2. Experimental

The feedstock Fe-base amorphous powder was produced by 80 h mechanical alloying (MA) of elemental powders. The mechanical alloying was performed in a high-energy planetary ball mill (Retch PM100) in argon atmosphere using hardened chromium steel vial and balls ($\Phi=20$ mm). The ball-to-powder weight ratio was 10:1 and the rotation speed of the main disc was kept around 280 rpm. The chemical composition of the alloy powder was 70Fe-15Cr-4Mo-5P-4B-1C-1Si (wt.%) which is equal to $\text{Fe}_{56}\text{Cr}_{13}\text{Mo}_{1.9}\text{P}_{7.2}\text{B}_{16.6}\text{C}_{3.7}\text{Si}_{1.6}$ (at.%). The MA powder was sprayed on a carbon steel substrate (50 by 50 by 5 mm) using HVOF (Metallisation Met JET II) system in three groups (HVOF-G1, HVOF-G2, and HVOF-G3) with different parameters as shown in Table 1. Substrates

Table 1 HVOF spraying parameters

Parameters	Microstructure		
	Amorphous (HVOF-G1)	Amorphous- nanocrystalline (HVOF-G2)	Nanocrystalline (HVOF-G3)
Oxygen gas flow rate, SLPM	833	682	560
Fuel (kerosene) flow rate, SLPM	0.37	0.21	0.14
Fuel/oxygen, Vol.%	0.044	0.031	0.025
Powder feed rate, g/min	35	35	35
Spray distance, mm	300	300	300
Scanning velocity, mm/s	50	50	50
Deposit thickness, μm	200	200	200
Nozzle length, mm	100	100	100
Compress air cooling	Yes	Yes	Yes

were cleaned prior to spraying by grit blasting with alumina grit (841 μm) on one side followed by ultrasonic cleaning in acetone to remove any grease and contaminations. To avoid significant heating during the HVOF process, the substrate was cooled on its backside using compressed air so the substrate temperature did not exceed over than 250 °C. Thick coatings of 200 μm were achieved in 2-3 passes.

X-ray diffraction (XRD: Philips XPERT-MPD) was performed to study the structural evolution of coatings. All XRD experiments were carried out in continuous scanning mode using Cu-K α radiation ($\lambda=0.1542$ nm) and 0.03° step size. Differential scanning calorimetry (DSC: NETZSCH DSC 404) with a constant heating rate of 20 K/min under flowing argon gas (99.999%) was used to study the crystallization behavior of amorphous coatings. The cross-sectional microstructures of coatings were investigated by scanning electron microscopy (SEM: Philips XL30SERIES). High resolution transmission electron microscopy (HRTEM) of coatings was carried out using a Jeol-JEM-2010 TEM at an accelerating voltage of 200 kV and resolution of 0.19 nm. To accomplish sample preparation, the coating was first sectioned with diamond saw and then mechanically thinned to about 100 μm with paper grinding. In second step the thickness of thinned layer was decreased to 5 μm by dimpling machine (Gatan dimple grinder 656). The final step was ion milling (Gatan ion polishing 691) to obtain a very thin layer of <100 nm.

The Vickers microhardness value was calculated as average of 10 measurements recorded on polished cross sections of the coatings under a 25 gf load, using Matsuzawa MAXT70 digital microhardness tester.

3. Results and Discussion

3.1 The Structure of Coating

Figure 1 illustrates the XRD patterns of mechanically alloyed Fe-Cr-Mo-P-B-C-Si feedstock powder and the as-sprayed HVOF coatings. The detailed structural evolution during MA is given elsewhere (Ref 20). The presence of halo on XRD pattern confirms that the

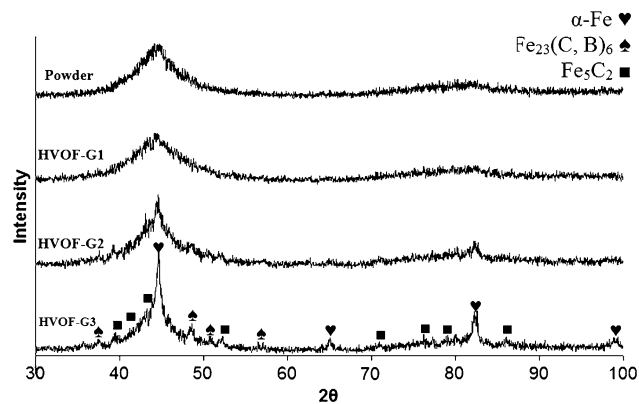


Fig. 1 XRD patterns of mechanically alloyed feedstock powder and Fe-Cr-Mo-P-B-C-Si HVOF coatings

feedstock MA powder used for HVOF spraying has an amorphous structure. As it can be seen in Fig. 2 each powder particle is an agglomerated cluster of many finer particles. The XRD pattern of HVOF-G1 coating in Fig. 1 also shows a halo characteristic indicating that this coating has an amorphous structure similar to feedstock MA powder. However, in HVOF-G2 there is an emergent crystalline peak on the top of the amorphous hub suggesting that this coating is a mixture of amorphous and crystalline phases. Structure of HVOF-G3 coating mainly consists of crystalline phases such as α -Fe, $Fe_{23}(C, B)_6$, and Fe_5C_2 .

It is inferred from the diffraction patterns that a full range of amorphous to fully crystalline microstructures can be obtained by adjusting of HVOF parameters especially fuel/oxygen ratio (see Table 1). Kishitake et al. reported that for Fe-17Cr-38Mo-4C gas atomized powder, amorphous coatings are obtained by the APS while a mixture of amorphous and crystalline phases are formed by HVOF (Ref 5, 6). They suggested that this difference may result from the difference of the cooling rate between the APS and HVOF processes. Cherigui et al. has shown that the structure of FeNb and FeSiB HVOF and APS coatings is partially amorphous (Ref 21). The feedstock powders that they used in their research were fully amorphous and were produced by mechanical alloying. Fenineche et al. found that the presence of some additive elements within the Fe-Cr-Mo matrix can promote amorphization (Ref 22). When the three empirical rules are applied to the present system, it is also composed of more than three types of elements, atomic size of the constituent elements decreases in the order of Mo > Si > P > Cr > Fe > B > C, and the heats of mixing are negative for the main atomic pairs (Ref 8). It is regarded that the alloy chosen here satisfies the three empirical rules for the stabilization of the supercooled liquid during HVOF spraying, leading to highly dense random packed atomic configurations, higher viscosity, and lower atomic diffusivity (Ref 8, 16) which is primarily attributed to the high GFA of Fe-Cr-Mo-P-B-C-Si system.

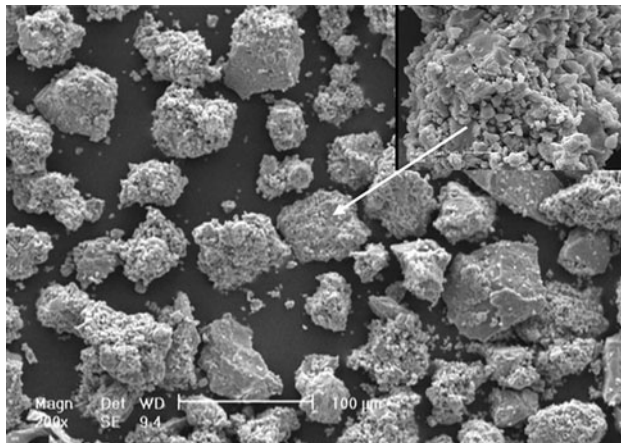


Fig. 2 SEM image of mechanically alloyed feedstock Fe-Cr-Mo-P-B-C-Si amorphous powders

The only way to increase the amount of amorphous phase by increasing the fuel/oxygen ratio is to go through a remelting to the liquid state followed by quenching to the amorphous state. Since the starting composition is the same in all three groups of coatings, the difference in the glassy fraction is related to the mechanism of the amount of cooling rate and remelting of individual particles in HVOF flame at various fuel/oxygen ratios. By increasing fuel/oxygen ratio, the flame temperature becomes too high and the velocity of the powder particles is much higher. Thus, the powder particles were completely remelted in the HVOF flame and then were rapidly solidified and quenched on the cold substrate forming an amorphous structure. By decreasing the fuel/oxygen ratio the particles did not remelt to a significant extent as well as the velocity of them becomes lower, thus the conditions appear to crystallize the amorphous feedstock powder in flame which explains the higher percentage of crystalline phase in the HVOF-G3 coatings.

3.2 Microstructural Observations

Figure 3 is the HRTEM image and selected area diffraction pattern (SADP) of mechanically alloyed powder after 80 h of milling, showing a fully amorphous microstructure, in accordance with the XRD patterns given in Fig. 1.

Typical SEM cross section image of HVOF coatings is shown in Fig. 4. As it can be seen, the microstructure of coatings includes very fine lamella structure which is smooth and dense, adhering well with the substrate with no cracking. Moreover, some pores are rarely observed in this microstructure as indicated by arrows can be seen from the images. The big pores located between flattened

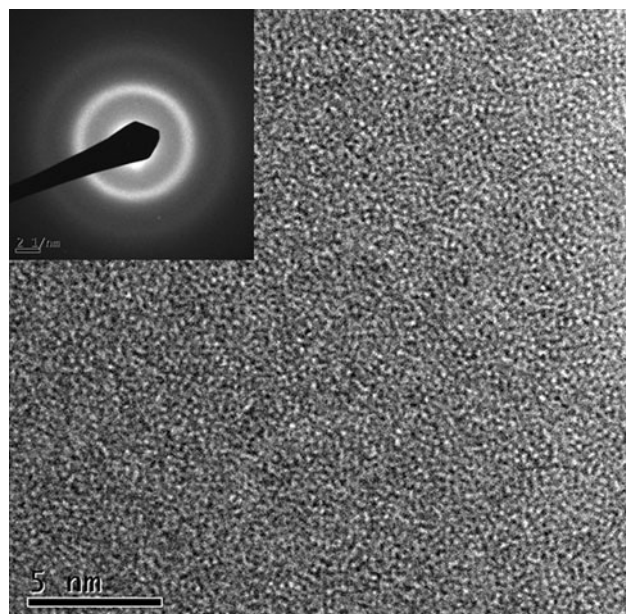


Fig. 3 HRTEM micrograph and SADP of mechanically alloyed feedstock Fe-Cr-Mo-P-B-C-Si amorphous powder

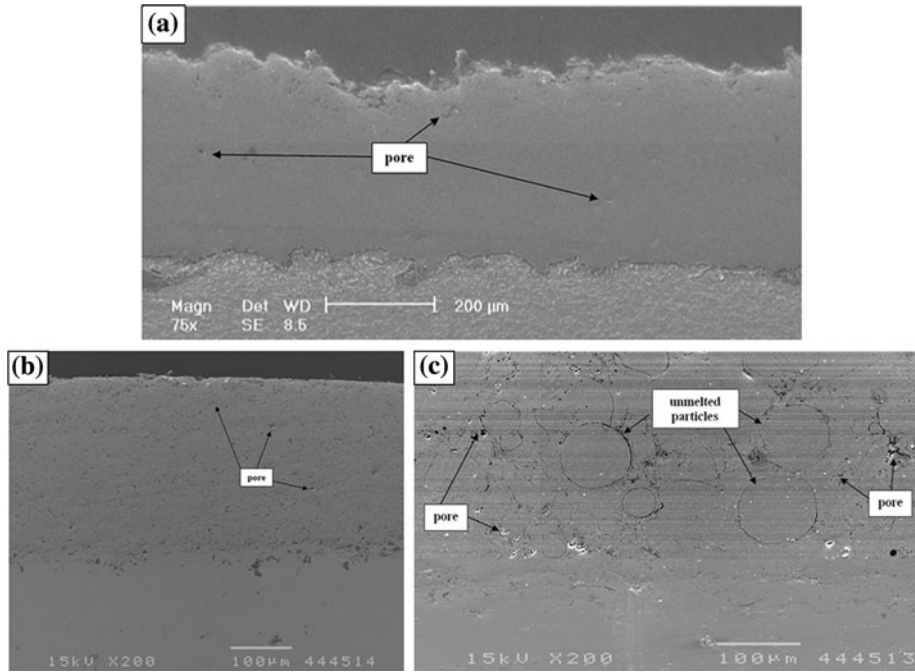


Fig. 4 SEM cross-sectional images of Fe-Cr-Mo-P-B-C-Si coatings (a) HVOF-G1, (b) HVOF-G2, and (c) HVOF-G3

droplets are mainly caused by the loose packed layer structure or gas porosity phenomenon, while the small pores within the flattened particles originate from the shrinkage porosity (Ref 23, 24). Obviously, the porosity of the coatings reduces in the order of HVOF-G3, G2, and G1, and it is believed that increasing the fuel/oxygen ratio, increases both the thermal and kinetic energy of the gas flow, so that the majority of the powder particles are better melted and also accelerated to higher velocities and deformed extensively on impact to form elongated lamella (Ref 25). Both factors contribute to making more tabular droplets to fill the interspaces of particles much more efficiently (Ref 26). In addition, the fine feedstock MA particles (Fig. 2) cooperated to make a fully dense and compact microstructure. Some unmelted particles are clearly visible in HVOF-G3 (Fig. 4c) coating because of lower flame temperature (minimum fuel/oxygen ratio) in this condition.

High resolution transmission electron microscopy was used in order to study the detailed microstructure of HVOF coatings. As expected a wide range of features are observed on TEM. HRTEM image has shown in Fig. 5 confirms that HVOF-G1 coating is completely amorphous. The amorphous structure in the as-sprayed coatings can be explained by the quenching of fully molten particles from their hottest temperature of flame (3000 °C for HVOF) through the impact onto the cold substrate surface leading to the suppression of nucleation (Ref 27, 28). As it can be seen in Table 1, this microstructure appears when the fuel/oxygen ratio has a maximum value.

As shown in Fig. 6 the HVOF-G2 coating consists of amorphous phase and nanocrystalline grains. The electron

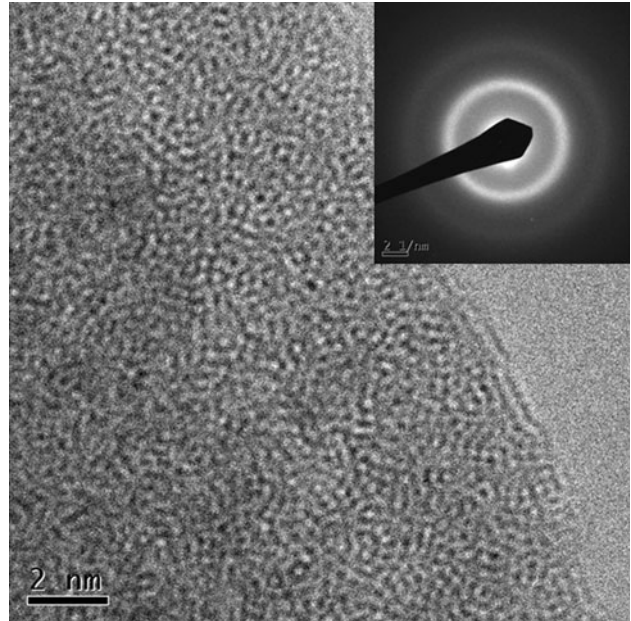


Fig. 5 HRTEM micrograph and SADP of amorphous Fe-Cr-Mo-P-B-C-Si HVOF coating (HVOF-G1)

diffraction pattern, in Fig. 6(a) was taken with the selected area aperture centered over the amorphous and nanocrystalline region and shows a diffuse amorphous halo with diffraction spots arising from nanocrystalline grains with a size range of 5-30 nm. The HRTEM micrograph and fast Fourier transform (FFT), as shown in Fig. 6(b), confirm the presence of a mixture of nanocrystalline grains

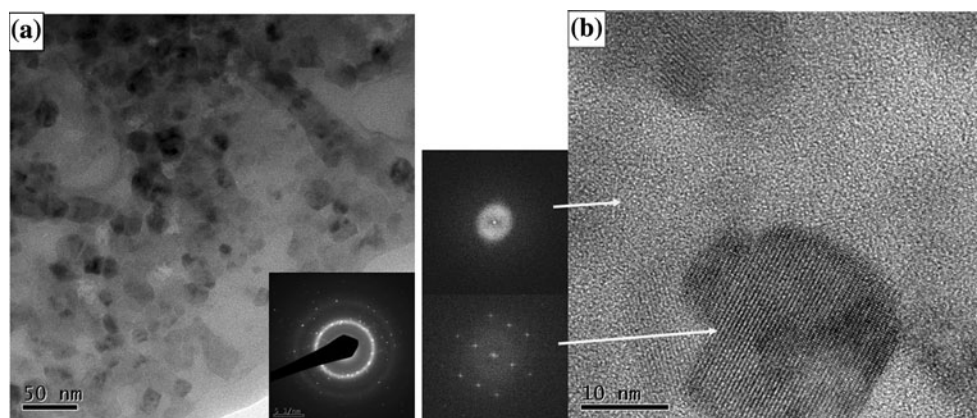


Fig. 6 (a) TEM and (b) HRTEM micrographs, SADP and FFT of amorphous-nanocrystalline Fe-Cr-Mo-P-B-C-Si HVOF coatings (HVOF-G2)

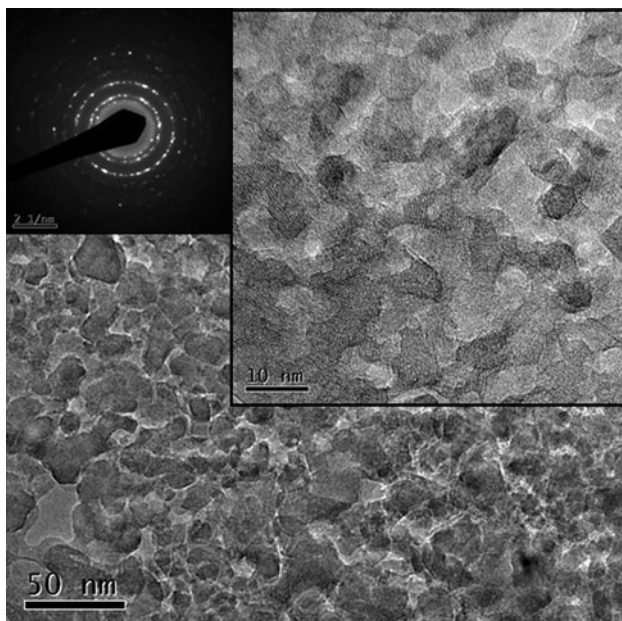


Fig. 7 TEM and HRTEM micrographs and SADP of nanocrystalline Fe-Cr-Mo-P-B-C-Si HVOF coating (HVOF-G3)

within an amorphous matrix. In this case the fuel/oxygen ratio is moderate (HVOF-G2) so this duplex microstructure can be explained by quenching of semi-molten particles when impinged to the cold substrate. Therefore, some unmelted particles crystallized inside the HVOF flame to yield nanocrystalline grains which embedded within the amorphous matrix.

A nanocrystalline structure with equiaxed grains was obtained in case of HVOF-G3 coating (Fig. 7). In this condition the fuel/oxygen ratio has a minimum value and the HVOF flame temperature is the lowest so the most of the individual powder particles were unmelted and crystallized inside the HVOF flame. Moreover, the cooling rate was sufficiently high to avoid grain coarsening and yielded nanocrystalline structure.

Table 2 Microhardness value of MA powder and Fe-Cr-Mo-P-B-C-Si HVOF coatings

Microstructure of coatings	Microhardness (HV ₂₅)	
	Mean	Standard deviation
Mechanical alloying powder	780	10.4
Amorphous (HVOF-G1)	830	36.4
Amorphous-nanocrystalline (HVOF-G2)	950	85.3
Nanocrystalline (HVOF-G3)	1230	46.2

3.3 Microhardness Value

The microhardness value of amorphous feedstock MA powder and HVOF coatings are given in Table 2. All the as-sprayed coatings revealed a high hardness of around 800 to 1200 HV. The value of hardness was similar to that of the bulk Fe-based metallic glass (Ref 29) but it was higher than that of electroplated chromium and the Ni-based amorphous coatings (Ref 9). The difference in hardness value of the three groups of HVOF coatings in this study is attributed mainly to the difference in volume fraction of amorphous and nanocrystalline phases. A fully amorphous coating has lower hardness (830 HV) compared to the duplex amorphous-nanocrystalline coating (950 HV). The fully nanocrystalline coating has the highest microhardness (1230 HV), probably due to precipitation of some carbides such as $\text{Fe}_{23}(\text{C}, \text{B})_6$ and Fe_5C_2 during crystallization. Some researchers suggested that the hardness of the amorphous Fe-base coating increases after crystallization (Ref 6, 30). In contrast Kishitake et al. reported that the duplex microstructure consisting of the both amorphous and nanocrystalline structure exhibits a higher hardness than fully amorphous or nanocrystalline structure (Ref 5). The difference is mainly attributable to the difference of decomposition of amorphous phase during crystallization.

3.4 Thermal Behavior

Figure 8 shows DSC curves for as-milled powder and HVOF coatings. As seen the crystallization of MA powder

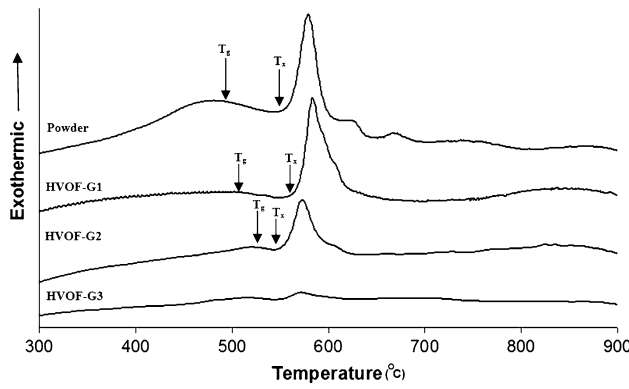


Fig. 8 DSC curves of mechanically alloyed feedstock powder and Fe-Cr-Mo-P-B-C-Si HVOF coatings

Table 3 Crystallization characteristics of Fe-Cr-Mo-P-B-C-Si HVOF coatings

Microstructure	T_x , °C	T_g , °C	ΔT_x , °C	T_p , °C	Amorphous percentage, %
Mechanical alloying powder	559.3	490	69.3	580.3	100
Amorphous (HVOF-G1)	566.3	499	67.3	584.3	100
Amorphous-nanocrystalline (HVOF-G2)	555.9	522	33.9	574.9	44
Nanocrystalline (HVOF-G3)	555.7	533	22.7	571.7	2.1

occurs in single stage around 560–580 °C. The exothermic peak at 550–580 °C is attributed to the crystallization of amorphous phase for HVOF coatings. The crystallization peak of amorphous-nanocrystalline coating (HVOF-G2) is smaller compared with that of the amorphous powder and coating (HVOF-G1) and shifted to lower temperature because of the change in composition of the remaining amorphous phase after crystallization. These results are in accordance with those reported by other researchers (Ref 4, 5, 15). The supercooled liquid region, ΔT_x , defined by the difference between the glass transition temperature (T_g) and the onset temperature of crystallization (T_x), is as large as 69 °C and summarized in Table 3. The ΔT_x value of the amorphous phase in the feedstock MA powder, amorphous coating (HVOF-G1) and amorphous-nanocrystalline coating (HVOF-G2) is in agreement with those of Fe-based bulk amorphous alloys reported by Inoue et al. (Ref 8, 29) and the Fe-based thick amorphous alloy coating studied by Wu and Hong (Ref 3, 17). It is suggested that a large ΔT_x generally represents a high GFA in the amorphous alloys (Ref 17, 31). By comparing the crystallization heat (obtained from the area under crystallization peak) on DSC curve of as-sprayed coating with that of fully feedstock MA amorphous powder, the amorphous volume fraction for the HVOF coatings was estimated as shown in Table 3 (Ref 14, 32).

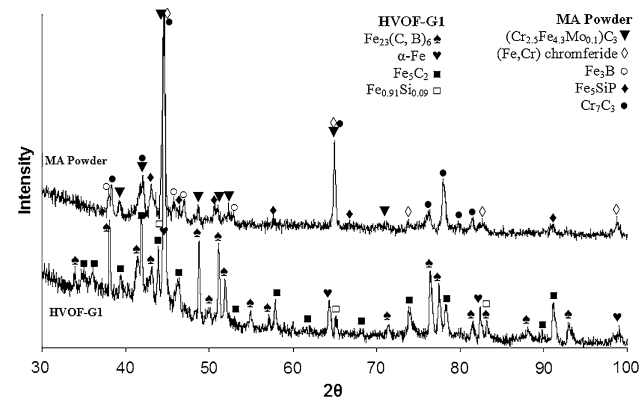


Fig. 9 XRD patterns of MA powder and HVOF-G1 coating after full crystallization in DSC run

Figure 9 shows the XRD pattern of MA powder and HVOF-G1 (fully amorphous structure) coating after DSC run. These results indicate that the single crystallization peak of both MA powder and HVOF-G1 is due to the simultaneous precipitation of crystalline carbide, boride, and α -Fe phase from amorphous structure. The difference in phase composition of HVOF-G1 coating and MA powder after DSC run is due to the rearrangement of elemental solid solution and amorphization of feedstock MA powder during HVOF thermal spraying.

4. Conclusions

HVOF spraying of mechanically alloyed amorphous Fe-Cr-Mo-P-B-C-Si powder was employed to obtain amorphous and nanocrystalline coatings. The hardness of the HVOF coatings depends on the volume fraction distribution of the amorphous and nanocrystalline content. The difference in the amorphous fraction of as-sprayed HVOF coatings is related primarily to the fuel/oxygen ratio. The individual powder particles with high GFA when exposed to HVOF flame temperatures with high fuel/oxygen ratio are completely melted and then rapidly quenched and solidified on the cold substrate to form a fully amorphous structure. While the fuel/oxygen ratio decreases (lower flame temperature), the powder particles become semi-molten, leading to the full or partial crystallization of powders within the HVOF flame. Thus, this work shows that HVOF is an efficient method to prepare a wide range of mixed amorphous/nanocrystalline structures for the Fe-Cr-Mo-P-B-C-Si alloy system.

Acknowledgment

The authors would like to thank Nanyang Technological University (NTU) for providing characterization equipments and Poudrafshan Company (PACO) for providing HVOF facilities.



References

1. Y.S. Kim, K.T. Kim, B.T. Kim, and J.I. Bae, Microstructure and Wear Behavior of Thermally Sprayed Fe-based Amorphous Coating, *Key Eng. Mater.*, 2007, **353-358**, p 848-851
2. A.L. Greer, K.L. Rutherford, and I.M. Hutchings, Wear Resistance of Amorphous Alloys and Related Materials, *Int. Mater. Rev.*, 2002, **47**(2), p 87-112
3. Y. Wu, P. Lin, G. Xie, J. Hu, and M. Cao, Formation of Amorphous and Nanocrystalline Phases in High Velocity Oxy-Fuel Thermally Sprayed a Fe-Cr-Si-B-Mn Alloy, *Mater. Sci. Eng. A*, 2006, **430**, p 34-39
4. K. Kishitake, H. Era, and F. Otsubo, Thermal-Sprayed Fe-10Cr-13P-7C Amorphous Coatings Possessing Excellent Corrosion Resistance, *J. Therm. Spray Technol.*, 1996, **5**(4), p 476-482
5. K. Kishitake, H. Era, and F. Otsubo, Characterization of Plasma Sprayed Fe-17Cr-38Mo-4C Amorphous Coatings Crystallizing at Extremely High Temperature, *J. Therm. Spray Technol.*, 1996, **5**(3), p 283-288
6. K. Kishitake, H. Era, and F. Otsubo, Characterization of Plasma Sprayed Fe-10Cr-10Mo-(C, B) Amorphous Coatings, *J. Therm. Spray Technol.*, 1996, **5**(2), p 145-153
7. M. Cherigui, Z. Salhi, N.E. Fenineche, P. Gougeon, and C. Coddet, FeSi HVOF Thermal Spray Coatings: Diagnostic, Microstructure, and Magnetic Properties, *Mater. Lett.*, 2005, **59**, p 463-467
8. S.J. Pang, T. Zhang, K. Asami, and A. Inoue, Synthesis of Fe-Cr-Mo-C-B-P Bulk Metallic Glasses with High Corrosion Resistance, *Acta Mater.*, 2002, **50**, p 489-497
9. H.S. Ni, X.H. Liu, X.C. Chang, W.L. Hou, W. Liu, and J.Q. Wang, High Performance Amorphous Steel Coating Prepared by HVOF Thermal Spraying, *J. Alloys Compd.*, 2009, **467**, p 163-167
10. L. Ajelsztajn, B. Jodoin, P. Richer, E. Sansoucy, and E.J. Lavigne, Cold Gas Dynamic Spraying of Iron-Base Amorphous Alloy, *J. Therm. Spray Technol.*, 2006, **15**(4), p 495-500
11. H.W. Jin, C.G. Park, and M.C. Kim, Microstructure and Amorphization Induced by Frictional Work in Fe-Cr-B Alloy Thermal Spray Coatings, *Surf. Coat. Technol.*, 1999, **113**, p 103-112
12. Q.F. Guan, P.L. Yang, H. Zou, and G.T. Zou, Nanocrystalline and Amorphous Surface Structure of 0.45% C Steel Produced by High Current Pulsed Electron Beam, *J. Mater. Sci.*, 2006, **41**, p 479-483
13. A.V. Sergueeva, N.A. Mara, D.J. Branagan, and A.K. Mukherjee, Phase Morphology Effect on Elevated Temperature Mechanical Behavior of Nanostructures, *Mater. Lett.*, 2007, **61**, p 1465-1468
14. D.J. Branagan, W.D. Swank, D.C. Haggard, and J.R. Fincke, Wear-Resistant Amorphous and Nanocomposite Steel Coatings, *Metall. Mater. Trans. A*, 2001, **32**, p 2615-2621
15. M. Cherigui, N.E. Fenineche, A. Gupta, G. Zhang, and C. Coddet, Magnetic Properties of HVOF Thermally Sprayed Coatings obtained from Nanostructured Powders, *Surf. Coat. Technol.*, 2006, **201**, p 1805-1813
16. A. Kobayashi, S. Yano, H. Kimura, and A. Inoue, Mechanical Property of Fe-base Metallic Glass Coating formed by Gas Tunnel Type Plasma Spraying, *Surf. Coat. Technol.*, 2008, **202**, p 2513-2518
17. X. Wu and Y. Hong, Fe-based Thick Amorphous-Alloy Coating by Laser Cladding, *Surf. Coat. Technol.*, 2001, **141**, p 141-144
18. A.V. Sergueeva, D.J. Branagan, and A.K. Mukherjee, Microstructure/Properties Relationship in Fe-based Nanomaterials, *Mater. Sci. Eng. A*, 2008, **493**, p 237-240
19. F. Otsubo, H. Era, and K. Kishitake, Formation of Amorphous Fe-Cr-Mo-8P-2C Coatings by the High Velocity Oxy-Fuel Process, *J. Therm. Spray Technol.*, 2000, **9**(4), p 494-498
20. B. Movahedi, "Microstructural and Tribological Evaluation of Novel Fe-based Amorphous-Nanocrystalline Thermal Spray Coatings," PhD Thesis, Isfahan University of Technology, 2010
21. M. Cherigui, N.E. Fenineche, and C. Coddet, Structural Study of Iron-based Microstructured and Nanostructured Powders Sprayed by HVOF Thermal Spraying, *Surf. Coat. Technol.*, 2005, **192**, p 19-26
22. N.E. Fenineche, M. Cherigui, H.I. Feraoun, H. Aourag, and C. Coddet, FeNb and FeSi Thermal Spraying Coatings: Microstructure and First Principle Calculations, *Mater. Sci. Eng. B*, 2004, **107**, p 27-32
23. V.V. Sobolev and J.M. Guilemany, Investigation of Coating Porosity Formation During High Velocity Oxy-Fuel (HVOF) Spraying, *Mater. Lett.*, 1994, **18**, p 304-308
24. T.C. Totemeier, Effect of High-Velocity Oxygen-Fuel Thermal Spraying on the Physical and Mechanical Properties of Type 316 Stainless Steel, *J. Therm. Spray Technol.*, 2005, **14**(3), p 369-372
25. G. Ji, O. Elkdim, and T. Grosdidier, Deposition and Corrosion Resistance of HVOF Sprayed Nanocrystalline Iron Aluminide Coatings, *Surf. Coat. Technol.*, 2005, **190**, p 406-416
26. Z. Zhou, L. Wang, F.C. Wang, H.F. Zhang, Y.B. Liu, and S.H. Xu, Formation and Corrosion Behavior of Fe-based Amorphous Metallic Coatings by HVOF Thermal Spraying, *Surf. Coat. Technol.*, 2009, **204**, p 563-570
27. J.M. Guilemany, J. Nutting, and M.J. Dougan, A Transmission Electron Microscopy Study of the Microstructures Present in Alumina Coatings Produced by Plasma Spraying, *J. Therm. Spray Technol.*, 1997, **6**(4), p 425-429
28. D.I. Shin, F. Gitzhofer, and C. Moreau, Properties of Induction Plasma Sprayed Iron Based Nanostructured Alloy Coatings for Metal Based Thermal Barrier Coatings, *J. Therm. Spray Technol.*, 2007, **16**(1), p 118-127
29. A. Kobayashi, S. Yano, H. Kimura, and A. Inoue, Fe-based Metallic Glass Coatings Produced by Smart Plasma Spraying Process, *Mater. Sci. Eng. B*, 2008, **148**, p 110-113
30. D.J. Branagan, M. Breitsameter, B.E. Meacham, and V. Belashchenko, High-Performance Nanoscale Composite Coatings for Boiler Applications, *J. Therm. Spray Technol.*, 2005, **14**(2), p 196-204
31. A. Basu, A.N. Samant, S.P. Harimkar, J.D. Majumdar, I. Manna, and N.B. Dahotre, Laser Surface Coating of Fe-Cr-Mo-Y-B-C Bulk Metallic Glass Composition on AISI, 4140 Steel, *Surf. Coat. Technol.*, 2008, **202**, p 2623-2631
32. C.R.M. Afonso, C. Bolfarini, W.J.B. Filho, and C.S. Kiminami, Spray Forming of Glass Former Fe63Nb10Al4Si3B20 Alloy, *Mater. Sci. Eng. A*, 2007, **449-451**, p 884-889